applied sciences

MDPI

Article

Perspective of Using Vertically Oriented Graphene as an Electrochemical Biosensing Platform

Elena Anghel [1,2,*], Bianca Adiaconita [3], Andrei Avram [3] and Ioana Demetrescu [2,4]

[1] Extreme Light Infrastructure—Nuclear Physics (ELI-NP), 30 Reactorului Street, 077125 Magurele, Romania
[2] Faculty of Chemical Engineering and Biotechnologies, University Politehnica of Bucharest, 1-7 Gheorghe Polizu Street, 011061 Bucharest, Romania; ioana.demetrescu@upb.ro
[3] National Institute for Research and Development in Microtechnologies—IMT Bucharest, 126A Erou Iancu Nicolae Street, 077190 Bucharest, Romania; bianca.tincu@imt.ro (B.A.); andrei.avram@imt.ro (A.A.)
[4] Academy of Romanian Scientists, 3 Ilfov Street, 030167 Bucharest, Romania
* Correspondence: elena.anghel@eli-np.ro

Abstract: Electrochemical sensors based on vertically oriented graphene (VG) have gained attention in recent years due to the unique properties of VG, such as its large surface area, biocompatibility, and high electrical conductivity. In this paper, we studied an electrochemical sensor with interdigitated electrodes modified with VG as an essential interface for the identification of two types of human colon adenocarcinoma cells: SW403 (high invasiveness) and HT29 (low invasiveness). Both cell lines have epithelial morphology, and we tested the electrochemical sensor on different concentrations of SW403 and HT29 cells. Scanning electron microscopy (SEM) and transmission electron microscopy (TEM) were used for morphological characterization of VG deposited on the working interdigitated electrodes, Raman spectroscopy was used to evaluate the graphitic nature of the VG growth on electrodes, and atomic force microscopy (AFM) was used to study the rugosity of the VG. Fourier-transform infrared spectrometry (FTIR) was used to study the configurations of the chemical bonds in the VG used for the working electrode of the electrochemical sensor. Vertically oriented graphene improves the sensor's response on the cell lines, as evaluated by electrochemical impedance spectroscopy (EIS).

Keywords: vertical graphene (VG); cell lines; sensor; EIS

check for updates

Citation: Anghel, E.; Adiaconita, B.; Avram, A.; Demetrescu, I. Perspective of Using Vertically Oriented Graphene as an Electrochemical Biosensing Platform. *Appl. Sci.* **2023**, *13*, 11833. https://doi.org/10.3390/app132111833

Academic Editors: Vittoria Guglielmi and Junseop Lee

Received: 22 September 2023
Revised: 16 October 2023
Accepted: 27 October 2023
Published: 29 October 2023

Copyright: © 2023 by the authors. Licensee MDPI, Basel, Switzerland. This article is an open access article distributed under the terms and conditions of the Creative Commons Attribution (CC BY) license (https://creativecommons.org/licenses/by/4.0/).

1. Introduction

Vertically oriented graphene (VG), also known as vertical graphene nanosheets (VGNs) or carbon nanowalls (CNW), is a unique form of graphene that is grown in a vertical orientation rather than the typical horizontal orientation [1,2]. This material has several unique properties that make it attractive for a variety of applications. First, the vertical orientation of the graphene nanosheets allows for better accessibility to the surface area, which can enhance its properties for use in energy storage and conversion, catalysis, and sensing applications [3,4]. Additionally, the vertical orientation can help prevent the agglomeration of the graphene sheets, a common issue in horizontally oriented graphene. One of the methods used to produce VG is plasma-enhanced chemical vapor deposition (PECVD), where a catalyst is used to facilitate the growth of the graphene sheets in a vertical orientation [4]. Depending on the intended application, the resulting material can be manipulated to form different shapes and sizes.

The combination of the shape and arrangement of VG has been of great interest to scientists from different disciplines. This adaptable material is created with carbon atoms organized in a honeycomb lattice, with one carbon atom at each hexagonal corner. As a two-dimensional sheet, it has excellent electrical, optical, and thermal properties [4]. When the three-dimensional form of VG is built up, its geometry can be influenced further to amplify its unique characteristics [5]. This vertical organization allows researchers to study

and exploit the properties of VG. Combining its inborn qualities with creative outside control will enable us to make diverse amalgam materials with various properties and applications [4,6].

Electrochemical detection is a widely used method for detecting target molecules. This is because it relies on measuring the changes at the electrode/electrolyte interface, which result from the conformational changes of the biorecognition between antibody and antigen [7]. VG enables the construction of high-performance and electrochemical biosensors by providing a robust signal capture and transduction platform. Specifically, it facilitates the sensitive identification and response to organic, inorganic, and cellular targets. Generally, sensors, biosensors, and electrochemical biosensors consist of a receptor and a transducer. The receptor is a material that interacts with the target molecules, creating selectivity toward them. The transducer is then responsible for converting the information into a measurable signal. This enables applications such as medical diagnostics and environmental monitoring [8,9].

Graphene-based materials are used in many applications for electrochemical detection. Some examples in this direction are presented in this section. Wang et al. demonstrated the application of nitrogen-doped graphene oxide in electrochemical biosensing. The nitrogen-doped graphene exhibited enhanced electrochemical performance, enabling sensitive and selective detection of biomolecules. GO's functional groups can be easily tailored for specific biomolecule immobilization, offering fine-tuned selectivity. VG's three-dimensional structure may enhance mass transport and improve accessibility for biomolecule binding, potentially leading to improved sensitivity [10]. Chen et al. developed a three-dimensional tubular array based on nitrogen-doped graphene for high-rate supercapacitors. The unique structure of the nitrogen-doped graphene array provided enhanced electrochemical properties, making it suitable for energy storage and sensing applications. VG's high surface area and unique architecture could lead to improved supercapacitor performance and potentially enhanced sensing capabilities. Other materials might excel in specific energy storage applications, while VG's combination of electrochemical and sensing properties could be advantageous [11]. Patiño et al. developed an electrochemical genosensing platform using graphene oxide to detect short DNA sequences related to a specific virus. The graphene oxide platform exhibited high sensitivity and selectivity, making it suitable for DNA sensing applications. GO's functionalization can create a suitable microenvironment for DNA hybridization and improve the stability of the sensor. VG's structure may offer an enhanced surface area for DNA immobilization and improved binding kinetics [12].

Many researchers in the field validate the advantages of using VG in developing sensors, and there are some examples that were described in detail in the previous work [4]. We mention some of them here. Mao et al. [13] pioneered a biosensor employing a vertical graphene field-effect transistor, demonstrating both sensitivity and selectivity. In 2017, Qianwei and colleagues harnessed VG to create an electrochemical biosensor for lactic acid monitoring [14]. Tzouvadaki et al. [15] utilized VG for ultrasensitive detection of etoposide, a chemotherapy drug. A portable electrochemical sensing device was developed for Alzheimer's biomarker detection using nanoAu-modified vertical graphene (VG@Au), boasting a linear range from 0.1 pg/mL to 1 ng/mL and a detection limit of 0.034 pg/mL for tau protein [16]. In an innovative study, Abolpour employed flexible VG electrodes to create a versatile flow sensor with applications in medical treatments, environmental monitoring, and motion detection [17]. Burinaru et al. introduced an electrochemical impedance spectroscopy biosensor in a microfluidic device for circulating tumor cell (CTC) detection [18]. Tincu et al. developed a biosensor with vertically aligned nanosheets and anti-EpCAM antibodies [19].

In this paper, we analyzed the advantages of the properties of vertical graphene grown at 700 °C [20] and studied the improvement in interdigitated gold electrodes modified with this type of VG by investigating the electric properties of the two lines of tumor cells (SW403 and HT29) at two concentrations using an electrochemical sensor with VG-based interdigitated work electrodes [19]. We prepared two different cell solution concentra-

tions (10^4 and 10^6 cells/mL). We detected them with the VG-based electrochemical sensor using the electrochemical impedance spectroscopy (EIS) method based on the study by Tincu et al. [19]. EIS data analysis aims to determine the nature of the processes occurring at the electrode and their characteristic parameters. Scanning electron microscopy and transmission electron microscopy were performed to investigate the morphology of the VG grown on the working electrodes of the device used. Raman spectroscopy was used to assess the quality of the deposited VG film and identify VG's vibrational mode. Atomic force microscopy was used to study the VG morphology and find details about the roughness. Fourier-transform infrared spectrometry (FTIR) was used to study the configurations of the chemical bonds in the vertical graphene used for the working electrode of the electrochemical sensor before and after the electrochemical experiments.

2. Materials and Methods

2.1. Synthesis of VG

We obtained VG using specialized equipment for carbon material growth known as the PlasmaPro100 model Nanofab 1000 (Oxford Instruments, Abingdon, UK). This equipment operates in plasma-assisted (PECVD) and thermal (CVD) modes. For the growth process of VG, we used the PECVD mode using capacitively coupled plasma in the range of 200 to 900 °C between two electrodes. VG was grown directly on the working electrodes of the electrochemical sensor using the following parameters: temperature of 700 °C, growth time of 1 h, 300 W RF power, and 300 mTorr pressure. The gas mixture for obtaining VG was Ar:CH_4 at a ratio of 190:10 sccm (standard cubic centimeter per minute). In a previous study, we analyzed the growth conditions of VG in order to find the best characteristics of VG for use in modifying the surface of an electrochemical sensor for different cell identification and characterization. The study's conclusion [20] was that VG grown at a temperature of 700 °C has the best characteristics.

The functionality of the VG-based electrochemical sensor was demonstrated by testing it on two human colon adenocarcinoma cell lines: SW403, which is a cell line with a high level of invasiveness, and HT29, which is a cell line with a low level of invasiveness. The cell lines were cultured using the protocol [19] in the mediums RPMI-1640 and Mc-Coy's 5A. We suspended the cells in potassium ferrocyanide solution $[Fe(CN)_6]^{3-/4-}$ and prepared two concentrations of each cell line: 10^4 and 10^6 cells/mL.

2.2. Characterization Methods

Raman spectroscopy was carried out using a high-resolution scanning near-field optical microscope (SNOM) equipped with an integrated Raman module (Alpha-SNOM 300S, Witec, Germany) operating at a 532 nm wavelength. The solid-state laser used for the study is diode-pumped and can generate a laser power of up to 145 mW. With a spot size of 1.0, the laser was directed onto the sample using two objectives: 50 x × and 100 x.

The SEM analysis was performed using an FEI NovaTM NanoSEM 630 microscope (FEI Company). We analyze VG in the top view to see the density of the deposited film and the quality of the covering on the substrate, as well as in the cross-section to see the height of the VG film and the grown nanowalls.

TEM analysis was performed on a Jeol Jem arm 200F microscope equipped with an EDS unit (JEOL USA Inc., Peabody, MA, USA). The sample was prepared by the cross-section method, mechanical thinning to approximately 30 microns, followed by ion thinning in a Gatan Pips machine at an ion beam acceleration voltage of 4 kV and an incidence angle of 7 degrees. A lower voltage of 2 kV was finally used to reduce the amorphous surface layer covering the specimen.

The topography of the VG was characterized by AFM using a Nano Wizard4BioScience AFM system (JPK Instruments AG, Berlin, Germany). A 10 µm × 10 µm area was scanned in the air using intermittent contact mode. Three regions were examined for VG and further processed using Gwyddion 2.49 software. Finally, the surface roughness (Rq) and root

mean square (RMS) roughness, representing the surface height standard deviation, were determined.

For Fourier-transform infrared spectrometry (FTIR), a Bruker Optics Tensor 27 spectrometer was used, equipped with ATR Platinium and a reflection holder. ATR Platinium contains a diamond crystal with a single reflection. All samples were traced after 64 scans, with a resolution of 4 cm^{-1}, on a spectral domain of 4000–400 cm^{-1}. VG was analyzed before and after the electrochemical experiments.

EIS analysis was performed using an Autolab PGSTAT204 equipped with an FRA32M electrochemical impedance spectroscopy module (METROHM AUTOLAB AG., Utrecht, The Netherlands) with a 0.01 V AV amplitude. The initial phase involved analyzing and modeling the collected data using the spectrometer software NOVA 2.1.5. The data were then processed, and the electrochemical impedance characterized the sensor. When a stimulus is applied to the cell, it impacts the cell membrane's permeability. This change in permeability is represented by the impedance, which reflects the conductance of the membrane in the microelectrode array area. The cells were characterized using electrochemical impedance spectroscopy, using a device developed within the project [19]. By applying a small electric voltage between the interdigitated working electrode and the auxiliary electrode, oxidation and reduction reactions occur, resulting in electron release and capture. The solid–liquid interface exhibits capacitor-like behavior, with the capacitance expanding as the interface size increases. This flattens the initial drop and decreases the contact angle.

3. Results and Discussions

3.1. Raman Spectroscopy

Raman spectroscopy can provide information on the graphitic structure and quality of VG. The G peak at around 1580 cm^{-1} and the 2D peak at around 2700 cm^{-1} indicate the film has a graphitic nature. Moreover, the appearance of the D peak at about 1350 cm^{-1} and the D+G peak at around 2910 cm^{-1} reflects the presence of defects in the graphitic structure. A multitude of defects result from disorderliness, which in turn is caused by numerous edge states, sp^3-bonded C-H species, a base layer composed of nanographite, and defects that are ion-induced due to plasma exposure during the growth of VG film.

The Raman spectrum of VG film obtained at 700 °C is represented in Figure 1 and shows the specific bands D, G, and 2D centered at D~1340 cm^{-1}, G~1568 $cm^{-1,}$ and 2D~2665 cm^{-1}, respectively. They are shifted from their usual positions. The I_D/I_G ratio is 1.17 and is still in the range of low defect density. Also, the I_{2D}/I_G ratio with a value of 0.58 indicates that the nanosheets are formed from a few graphene layers. The importance of FWHM for D and G shows some defects in the crystalline lattice of the graphene due to nucleation centers. The analysis confirmed the specific bands of VG and its crystallinity, with some structural defects.

3.2. SEM and TEM Analysis

The typical structure of the VG, characterized by raised walls and ridge profiles, is visible in the SEM analysis (Figure 2a,b). The height of the walls measures approximately 500 nm in cross-section, and the growth rate of the VG is 9.16 nm/min. The VG film appears uniform with slight densification. In a previous study [20], distinct sheets of VG can be observed at temperatures between 600 °C and 700 °C. As the temperature increases, these sheets' deposition rate and interlacing become more pronounced. Beyond 750 °C, the VG layer becomes more compact, with densely packed sheets. The temperature of the substrate plays a crucial role in the PECVD process as it dramatically affects the surface reaction kinetics. A higher substrate temperature increases nucleation sites, promoting VG growth rate. Additionally, higher temperatures promote the formation of secondary nucleation sites on the VG sheets, contributing to increased interlinking at the active edges.

D (cm^{-1})	G (cm^{-1})	2D (cm^{-1})	D+G (cm^{-1})	I_D/I_G	I_{2D}/I_G	FWHM D (cm^{-1})	FWHM G (cm^{-1})
1340	1572	2667	2905	1.17	0.58	55	62

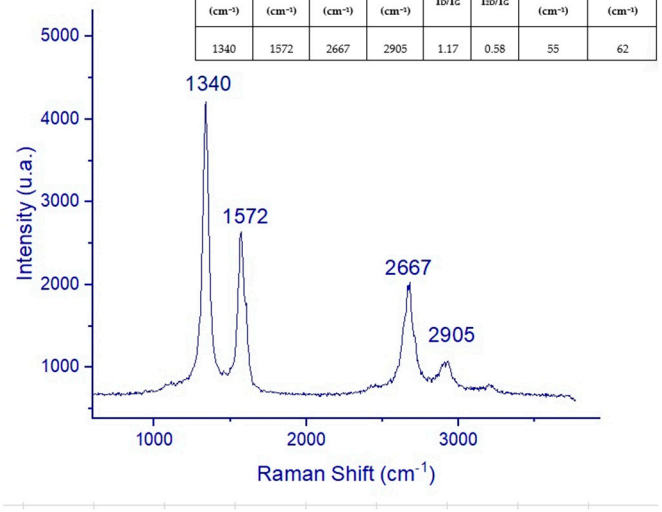

Figure 1. Raman spectrum of VG and table with Raman parameters.

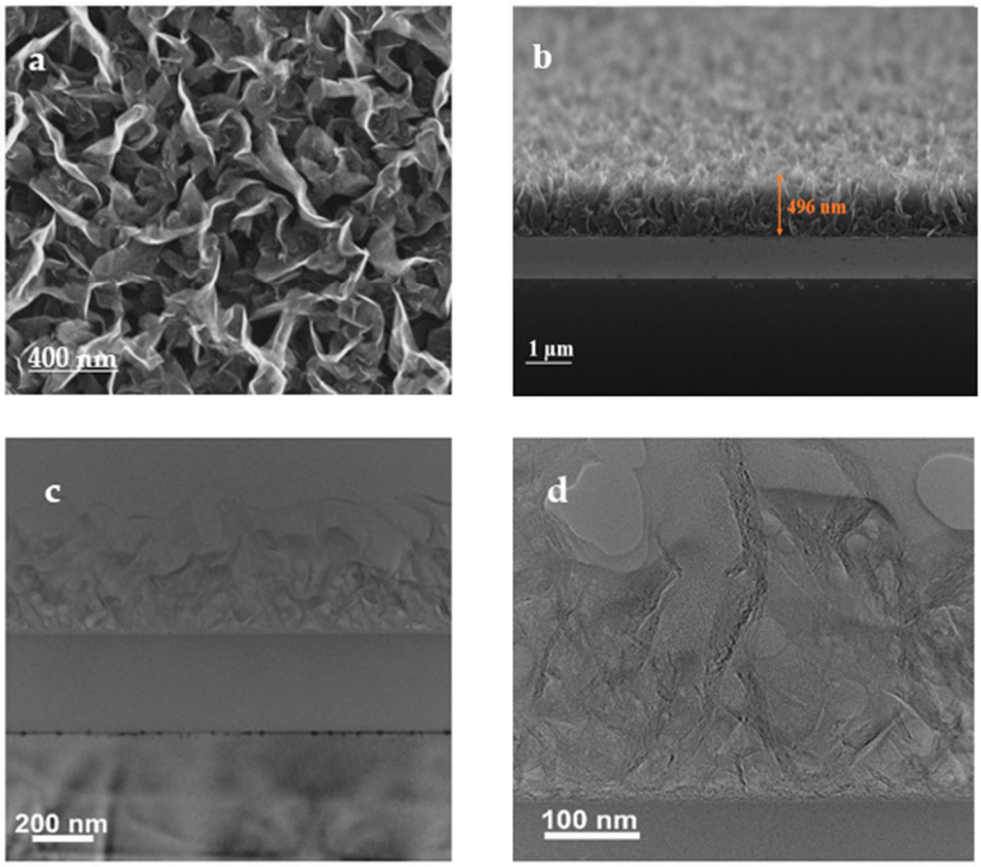

Figure 2. SEM images of VG film: (**a**) top-view of VG, (**b**) cross-section of VG and TEM images of VG film, (**c**) cross-section at 200 nm, and (**d**) cross-section at 100 nm.

Usually, in a TEM image, vertical graphene appears as a series of overlapping graphene layers, which their characteristic hexagonal honeycomb structure can identify. The quality of the VG can be evaluated from the TEM image by examining the morphology of the graphene layers. High-quality VG exhibits uniform interlayer spacing and a clean, smooth edge morphology [21]. Defects in graphene films, such as creases, folds, and dislocations, can also be observed in the TEM image, providing information on the material's growth process and mechanical properties.

As in the case of the SEM images (Figure 2a,b), the specific morphology of the vertical graphene can be observed in the TEM images (Figure 2c,d) of vertically oriented graphene walls and peaks of different sizes and heights. The SEM and TEM analyses are correlated. This morphology of VG on electrodes allows cell attachment and detection. VG has a high surface area, which provides cell attachment and interaction. Another characteristic is biocompatibility. As we saw in our article [20], based on fluorescence microscopy, the density of the U251 glioblastoma cells is higher on the VG surface, and the absorbance is about 1.138 µm, which involves the viability of the cells.

3.3. AFM Analysis

The surface roughness of VG can be interpreted by analyzing data obtained from scanning the surface with an atomic force microscope (AFM) presented in Figure 3. Roughness refers to surface variations in height, and AFM analysis can provide detailed information about these variations. With the help of AFM analysis, the topography of the surfaces of the vertical graphene samples was carried out, and the roughness was determined for the sample.

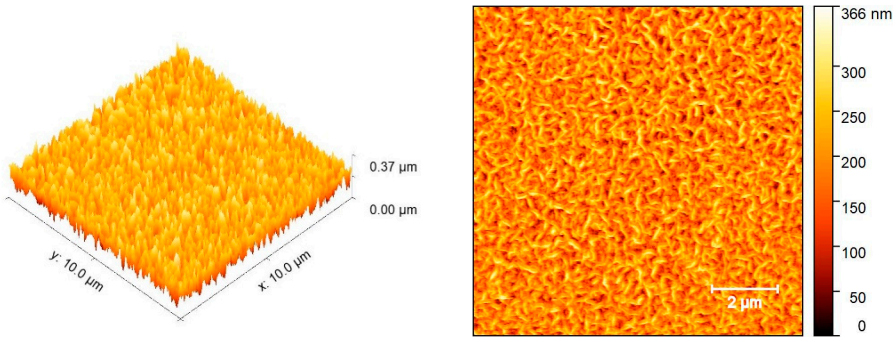

Figure 3. AFM micrography of VG.

The roughness of a sample refers to the asperities and variability in the surface relief of that sample. It measures the level of unevenness or irregularity of the surface. The roughness is characterized by the difference in the height of the points on the surface in relation to a reference plane. R_{MS} and R_q are two standard parameters used to quantify surface roughness in topographic analysis by AFM. These parameters are used to measure the average roughness and the variation in roughness on the analyzed surface. The value of R_{MS} is 48.32 $\pm$ 1.31 nm, and the value of R_q is 39.33 $\pm$ 1.10 nm. The result of the AFM analysis of the vertical graphene is correlated with the images obtained from the SEM analysis. The fact that vertical graphene has a high roughness indicates that its structure consists of vertical graphene walls with different heights. Some intertwine, giving it open edges with sharp tips and presenting irregularities on top. This characteristic offers an advantage regarding cell adhesion on the VG surface because the cells can adhere to the VG walls.

3.4. FTIR Analysis

Figure 4 shows the FTIR spectrum of VG grown on the silicon/silicon oxide substrate (violet spectrum). In the spectrum of the vertical graphene obtained after a PECVD process, no peaks can be observed that can be attributed to some functional groups. The peaks observed in the sample spectrum can be attributed to CO_2 molecules (2400–2200 cm^{-1}) and O-H bonds from the water molecules absorbed by the carbonaceous material (4000–300 and 1900–1200 cm^{-1}). The peaks at around 620 cm^{-1} can be attributed to the vibration mode of the Si-Si bonds in the wafer on which the VG was grown. Also, a film of SiO_2 is observed due to the appearance of peaks of reduced intensity in the 1200–1000 cm^{-1} region.

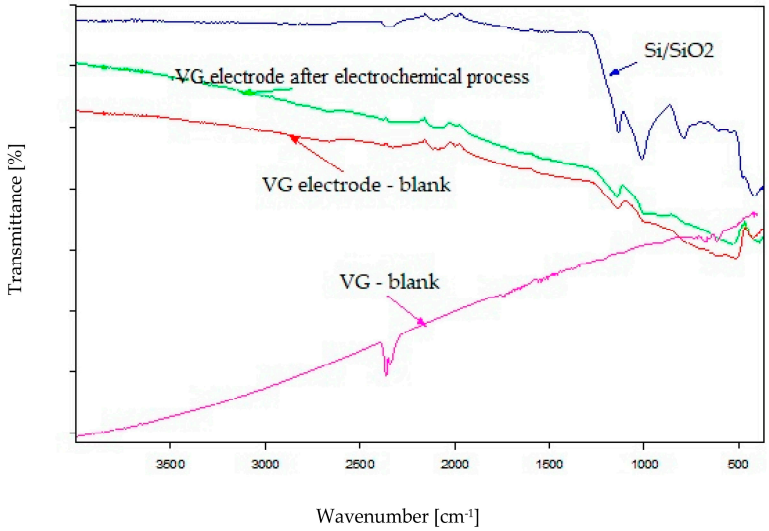

Figure 4. FTIR spectra for VG grown on the working electrode before and after the electrochemical processes.

Also, Figure 4 compares the spectra of the VG grown on the working electrode before (red spectrum) and after the electrochemical processes (green spectrum). A similarity between the two spectra can be observed, confirming the maintenance of the structural properties of the VG regarding electrochemical processes. No contamination of the film is observed after the stages of the EIS steps. As can be seen from the VG-blank spectrum, graphene does not show IR (infrared) bands, so it can be said that the spectra of the two samples are characterized by absorption bands that can be attributed to the substrate. In the 1200–400 cm^{-1} range, peaks can be observed that can be attributed to the Si-O bonds in the SiO_2 film and Si-Si in the silicon wafer. The peaks in the 2200–2000 cm^{-1} region can be assigned to SiHx bonds. Also, the FTIR image has a spectrum for the Si/SiO_2 substrate (blue spectrum).

The FTIR analysis confirmed that VG is not affected by the electrochemical processes involved in the EIS method. Both spectra of VG before and after the EIS measurements are almost identical, with the same peaks. This analysis concludes that VG maintained its properties after the EIS characterization.

3.5. EIS Analysis

The VG-based sensor [19], integrated into a microfluidic system and developed within the Research and Development Institute for Microtechnologies—IMT Bucharest, is made on a monocrystalline silicon wafer and consists of 2 interdigitated working microelectrodes on the surface of which vertical graphene is deposited at a temperature of 700 °C, each with 64 digits, a reference electrode, and an auxiliary electrode. The microfluidic system is made half on the chip with the sensor and the other half on a Corning 7740 glass chip, which is also the device's cover.

Applying a stimulus to the cells leads to a change in the permeability of the cell membrane—the result in impedance models the conductance of the membrane in the area of the microelectrode array. The characterization of the cells using the device [19] was carried out by electrochemical impedance spectroscopy. When applying an electric voltage between the interdigitated working electrode based on vertical graphene and the auxiliary electrode of several tens of mV, an oxidation reaction occurs with the release of electrons on the digits of one of the electrodes, the anode. On the digits of the other, a reduction reaction with electron captures and the solid–liquid interface behaves as a capacitor. The larger the interface, with the capacity to grow, the more a flattening of the initial drop, respectively, decreases the contact angle.

We conducted the EIS analysis to illustrate the electrical characteristics of adenocarcinoma cells, including the processes occurring at the VG electrode and the associated characteristic parameters. It can be seen from the Nyquist diagram that HT29 cells, compared to SW403, have lower electrical charge transfer resistance and higher electrical permittivity and conductivity. HT29 tumor cells have a highly folded membrane surface due to microvilli and, therefore, have a much larger cell surface than cells in the SW403 line. HT29 has a higher membrane capacity and a lower capacitive reactance. The higher membrane capacitance of HT29 cells results in storing more electrical charges, leading to higher conductivity and lower charge transfer resistance. At the microvilli level, lipid bridges have a very high concentration, especially cholesterol-ol-glycosphingolipids. If the surface area of HT29 cells is much larger compared to SW403, it means that the concentration of lipid bridges, that is, cholesterol-ol-glycosphingolipids, is also much higher. Therefore, tumor cells from the SW403 line adhere and form large cell conglomerates.

The variation curves in Figure 5a,b for SW403 (b) look different from those for HT29 (a) because the SW403 cells agglomerate to form large conglomerates. The Nyquist diagram (Figure 5) shows the capacitive reactance (imaginary impedance) as a function of the real impedance for two different concentrations (10^4 cells/mL and 10^6 cells/mL) for, respectively, HT29 and SW 403 cells. From the semicircular curve corresponding to high frequencies, the resistance can be determined using charge transfer (R_{ct}) and the capacity of the electric double layer (C_{dl}) that appears on the surface of the membrane. Still, it is also possible to determine the impedance modulus corresponding to the impedance resonance, the maximum of the semicircular curve. The linear variation in the imaginary impedance as a function of the real impedance related to low frequencies is due to Warburg diffusion.

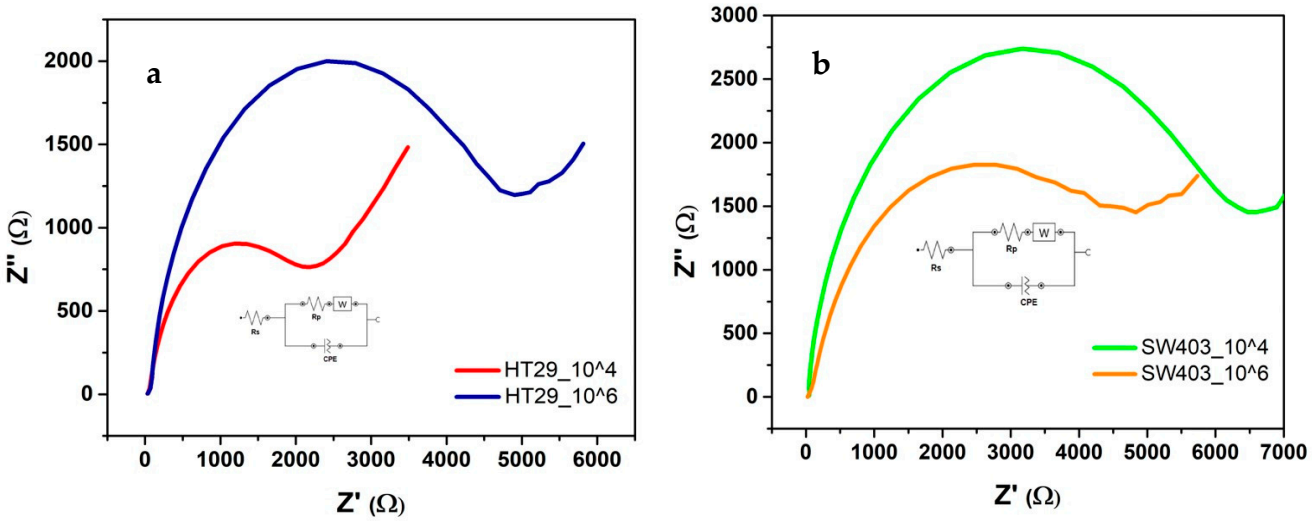

Figure 5. Nyquist diagram: (**a**) Concentration of 10^4 cells/mL and 10^6 cells/mL for HT29 cells and (**b**) Concentration of 10^4 cells/mL and 10^6 cells/mL for SW403 cells.

Electrical permittivity is inversely proportional to impedance and describes the ability of cells to resist an electric field. It decreases with increasing frequency when conductivity rises. The permittivity of polarized cells in the frequency range of 100 mHz–1 MHz is divided into two regions. The α dispersion region is defined below 100 kHz and represents the polarization of ions in a conductive medium. The β region, defined between 100 kHz and 1 MHz, is represented by the results from the build-up of charge at cell membranes due to the Maxwell–Wagner effect. In the Figures 6 and 7 are presented the variation of complex electrical permittivity for SW403 and HT 29 at the two concentrations: 10^4 and 10^6 cells/mL.

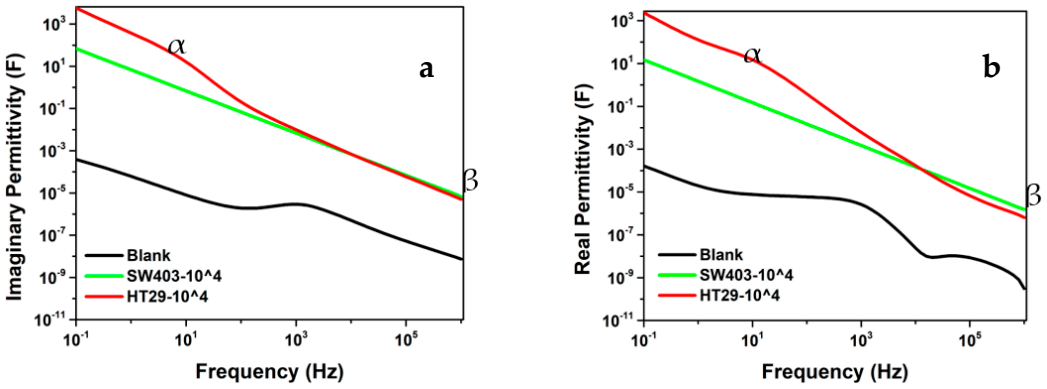

Figure 6. Variation in complex electrical permittivity for SW403 and HT29 at 10^4 cells/mL concentration: (**a**) imaginary permittivity and (**b**) real permittivity.

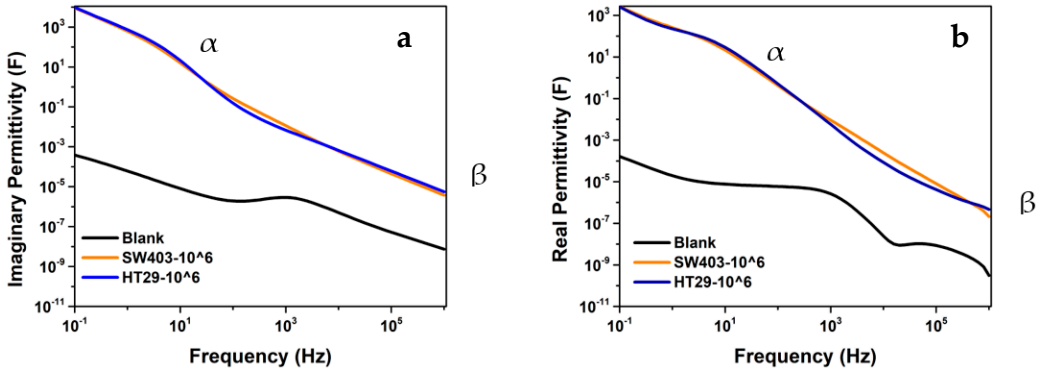

Figure 7. Variation in complex electrical permittivity for SW403 and HT29 at 10^6 cells/mL concentration: (**a**) imaginary permittivity and (**b**) real permittivity.

Complex permittivity measurements can help characterize and monitor tumor cells. The applied electric field will interact with the ions in the conductive medium, determining the alignment of the ions around the cell and causing interfacial polarization. Applications of high potential can permeabilize the cell membrane. That is why low potentials of the order of tens of mV are applied to measure cell impedance.

In Table 1, we can see the extracted impedance parameters found by fitting the impedance measured experimentally. The sample of SW 403 at a concentration of 10^4 cells/mL has the highest charge transfer resistance, R_{ct} = 3250 Ω, and the conductivity is lower, C_{dl} = 6.38 μF, than the sample of SW 403 at a concentration of 10^6 cells/mL (C_{dl} = 8.92 μF) but higher than HT 29 (C_{dl} = 5.66 μF and 4.85 μF, respectively) and blank VG (C_{dl} = 5.98 μF). The explanation for these parameters is that SW 403 forms large cell conglomerates that impede the current's passage.

Table 1. Impedance parameters.

Sample	R_s (Ω)	R_p (Ω)	R_{ct} (Ω)	Z''_{max} (Ω)	C_{dl} (μF)
VG	53.8	2630	1474	1237	5.98
SW 403—10^4 cells/mL	32.8	6071	3250	2921	6.38
HT 29—10^4 cells/mL	49.9	4071	1190	905	5.66
SW 403—10^6 cells/mL	29.9	5236	2787	1825	8.92
HT 29—10^6 cells/mL	39.4	5380	2409	1999	4.85

When tumor cells were captured on the electrode, the electron transfer at the electrode–molecule interface was obstructed, allowing for the measurement of tumor cells through

changes in impedance. This was evaluated using electrochemical impedance spectroscopy and can be observed from the Nyquist plot. The Faraday impedance in the electrical circuit consists of two components for charge transfer control and diffusion control: the Warburg impedance (W) and the electrode polarization resistance (Rp). The solution resistance (Rs) and the double-layer capacitance (Cdl) are ideal circuit elements. Rp and W are not exemplary components; they have a particular relationship with the measurement frequency.

The interaction of cells with the local electric field can cause the separation of charges and the creation of new dipoles, known as induced polarization. In biological systems, there are two important examples of induced polarization. One is the movement of ions on the surface of macromolecules due to the electric field, and the other is the interfacial polarization known as Maxwell–Wagner polarization on non-conducting surfaces. Biomaterials are made up of molecules with varying permittivity and conductivity. When an electric field is applied to these materials, the mobility of charge carriers, such as ions, is higher in certain areas (e.g., aqueous phases) than in others (e.g., lipid phases). This leads to a non-uniform distribution of charges on surfaces that are non-conductive. These heterogeneous systems have properties strongly dependent on frequency and differ from the properties of the individual phases.

As seen in Table 1, HT 29 cells have a lower resistance to charge transfer than SW 403 cells, which means that this cell line is more electrically conductive. HT 29 cells have microvilli on their surface, which is advantageous when passing the electric current. Moreover, the SW 403 cells form large conglomerates, so the resistance to charge transfer is higher and the electrical conductivity is lower.

Also, from the permittivity graphs (variation in complex permittivity), HT 29 is more conductive than SW 403 in the case of 10^4 cells/mL concentration. The real and imaginary permittivity values are higher than SW 403, and for the concentration of 10^6 cells/mL, they are similar for both cell lines.

SW 403 and HT 29 may have variations in their cell membrane composition and the types and densities of transport proteins. These transport proteins, such as ion channels and transporters, play a crucial role in controlling the movement of ions and molecules across the cell membrane. Variations in the expression and activity of transport proteins can lead to differences in ion permeability and distribution across the cell membrane. This, in turn, affects the overall electrical properties of the cell, contributing to impedance changes. For instance, variations in potassium, sodium, or chloride ion channels can alter the electrical conductivity and impedance of the cell membrane.

4. Conclusions

By correlating all of the characterization methods presented in this work, we can comprehensively understand vertical graphene's structural, morphological, chemical, and electrochemical properties. The results obtained from Raman spectroscopy, SEM analysis, TEM analysis, AFM, FTIR, and EIS collectively demonstrate the suitability of vertical graphene for use in electrochemical sensors, highlighting its potential for enhanced sensing performance, high surface area, efficient charge transfer, biocompatibility, and stability.

The HT 29 cells, compared to SW 403, have lower electrical charge transfer resistance and higher electrical permittivity and conductivity. Also, HT29 tumor cells have a highly folded membrane surface due to microvilli and, therefore, have a much larger cell surface than cells in the SW403 line. HT29 has a higher membrane capacity and a lower capacitive reactance. Its higher membrane capacitance stores more electrical charges, leading to a lower charge transfer resistance and higher conductivity.

Cells exhibit a dielectric signature that reflects their response to electromagnetic fields at various frequencies. This response is influenced by interactions between the electromagnetic fields and the molecules within the cellular membrane. The presence of VG on gold electrodes enhances the interface between the electrodes and the biomolecules, resulting

in increased biodetection surface and electrode conductivity. VG, a carbon nanomaterial, possesses higher electron mobility, making it a suitable choice for this modification.

The electrochemical analysis demonstrated the effectiveness of the VG-modified electrochemical sensor in detecting tumoral cells on the electrode surface at concentrations of 10^4 and 10^6 cells/mL. The EIS results showed that the HT 29 cell line had a larger cell membrane surface and lower capacitive reactance than the SW 403 cell line. The HT 29 cells had a higher conductivity and lower resistance to charge transfer due to their larger capacity to store electrical charges. This was attributed to many lipidic bonds at the microvilli, particularly cholesterol-ol-glycosphingolipids. Moreover, the SW 403 cells adhered and formed large cellular conglomerates, while the HT 29 cells had a higher conductive surface and experienced superior dielectric losses through conduction, as confirmed by the EIS measurements.

The observed decrease in Rct with an increase in tumor cell concentration is a complex outcome of these interacting factors. It is not solely due to electron obstruction but because of the dynamic interplay between the tumor cells and the electrochemical processes at the electrode surface. This phenomenon provides valuable insights into the behavior of tumor cells in our experimental system.

Author Contributions: Conceptualization and writing—original draft, E.A. and B.A.; review & editing, E.A., B.A., I.D. and A.A.; investigation, E.A. and B.A.; funding acquisition, E.A., I.D. and A.A. All authors have read and agreed to the published version of the manuscript.

Funding: This research was funded by the European Social Fund from the Sectoral Operational Programme Human Capital 2014-2020, Contract No. 13530/16.06.2022—SMIS Code: 153734.

Acknowledgments: We kindly acknowledge C. Pachiu from the National Institute for Research and Development in Microtechnologies—IMT Bucharest for the Raman spectrum of VG, O. Tutunaru from the National Institute for Research and Development in Microtechnologies—IMT Bucharest for the SEM image of VG, C. Istrate from the National Institute of Material Physics—Romania for the TEM image of VG, M. Bacalum from Horia Hulubei National Institute for R&D in Physics and Nuclear Engineering for the AFM topography of VG, and V. Tucureanu from the National Institute for Research and Development in Microtechnologies—IMT Bucharest for the FTIR spectrum of VG. This work was supported by the European Social Fund from the Sectoral Operational Programme Human Capital 2014-2020, through the Financial Agreement with the title "Training of PhD students and postdoctoral researchers in order to acquire applied research skills—SMART", Contract No. 13530/16.06.2022—SMIS Code: 153734.

Conflicts of Interest: The authors declare no conflict of interest.

References

1. Junhong, C.; Zheng, B.; Ganhua, L. *Vertically-Oriented Graphene: PECVD Synthesis and Applications*, 1st, ed.; Springer: Cham, Switzerland, 2015. [CrossRef]
2. Cao, X.; Shi, Y.; Shi, W.; Lu, G.; Huang, X. Vertically oriented graphene materials: Synthesis, characterizations, and applications. *Small* **2017**, *13*, 1701976.
3. Zhang, Y.; Wang, X.; Wu, H.; Zhou, C. Vertically oriented graphene-based materials: Synthesis, characterization, and applications. *Adv. Mater.* **2015**, *27*, 7493–7527.
4. Anghel, E.; Adiaconita, B.; Demetrescu, I.; Avram, A. A Review of Vertical Graphene and Its Biomedical Applications. *Coatings* **2023**, *13*, 761. [CrossRef]
5. Ren, J.; Han, J.; Ma, Y.; Wang, M.; Tong, Z.; Suhr, J.; Xiao, L.; Jia, S.; Chen, X. Morphology and surface engineering of vertical graphene films for dye photodegradation. *Ceram. Int.* **2022**, *48*, 9477–9482. [CrossRef]
6. Zheng, W.; Zhao, X.; Fu, W. Review of Vertical Graphene and its Applications. *ACS Appl. Mater. Interfaces* **2021**, *13*, 9561–9579. [CrossRef] [PubMed]
7. Ih, C.; Lee, J.; Kim, J.; Kang, M.S.; Paik, J.K.; Ku, S. Current technologies of electrochemical immunosensors: Perspective on signal amplification. *Sensors* **2018**, *18*, 207.
8. Bahamonde, J.P.; Nguyen, H.N.; Fanourakis, S.K.; Rodrigues, D.F. Recent advances in graphene-based biosensor technology with applications in life sciences. *J. Nanobiotechnol.* **2018**, *16*, 75.
9. Liu, A.; Wang, K.; Weng, S.; Lei, Y.; Lin, L.; Chen, W. Development of electrochemical DNA biosensors. *Trends Anal. Chem.* **2012**, *37*, 101–111. [CrossRef]

10. Wang, Y.; Shao, Y.; Matson, D.W.; Li, J.; Lin, Y. Nitrogen-doped graphene and its application in electrochemical biosensing. *ACS Nano* **2010**, *4*, 1790–1798. [CrossRef]
11. Chen, L.F.; Zhang, X.D.; Liang, H.W.; Kong, M.G.; Cui, Z.D.; Png, R.Q.; Chen, P. High performance three-dimensional tubular array based on nitrogen-doped graphene for high-rate supercapacitors. *ACS Nano* **2012**, *6*, 9132–9141.
12. Patiño, T.; Souto DE, P.; Lopes JM, J.; Chaves, A.R.; Machado SA, S.; Kubota, L.T. Electrochemical genosensing platform based on graphene oxide for detection of short DNA sequences related to the human T-cell lymphotropic virus. *Sens. Actuators B Chem.* **2018**, *254*, 808–814.
13. Mao, S.; Yu, K.; Chang, J.; Steeber, D.A.; Ocola, L.E.; Chen, J. Direct Growth of Vertically-oriented Graphene for Field-Effect Transistor Biosensor. *Sci. Rep.* **2013**, *3*, 1696. [CrossRef]
14. Chen, Q.; Sun, T.; Song, X.; Ran, Q.; Yu, C.; Yang, J.; Feng, H.; Yu, L.; We, D. Flexible electrochemical biosensors based on graphene nanowalls for the real-time measurement of lactate. *Nanotechnology* **2017**, *28*, 315501. [CrossRef]
15. Tzouvadaki, I.; Aliakbarinodehi, N.; Pineda, D.D.; De Micheli, G.; Carrara, S. Graphene nanowalls for high-performance chemotherapeutic drug sensing and anti-fouling properties. *Sens. Actuators B Chem.* **2018**, *262*, 395–403. [CrossRef]
16. Li, Y.; Liu, X.; Li, M.; Liu, Q.; Xu, T. Portable Vertical Graphene@Au-Based Electrochemical Aptasensing Platform for Point-of-Care Testing of Tau Protein in the Blood. *Biosensors* **2022**, *12*, 564. [CrossRef] [PubMed]
17. Abolpour, M.; Azadi, S.; Belford, A.; Razmjou, A.; Wu, S.; Han, Z.; Asadnia, M. Development of an Ultra-Sensitive and Flexible Piezoresistive Flow Sensor Using Vertical Graphene Nanosheets. *Nano-Micro Lett.* **2020**, *12*, 109. [CrossRef] [PubMed]
18. Burinaru, T.; Adiaconita, B.; Avram, M.; Preda, P.; Enciu, A.M.; Chiriac, E.; Marculescu, C.; Constantin, T. Electrochemical impedance spectroscopy based microfluidic biosensor for the detection of circulating tumor cells. *Mater. Today Commun.* **2022**, *32*, 104016. [CrossRef]
19. Tincu, B.; Burinaru, T.; Enciu, A.M.; Preda, P.; Chiriac, E.; Marculescu, C.; Avram, M.; Avram, A. Vertical Graphene-Based Biosensor for Tumor Cell Dielectric Signature Evaluation. *Micromachines* **2022**, *13*, 1671. [CrossRef]
20. Anghel, E.; Adiaconita, B.; Avram, A.; Mihailescu, C.; Pachiu, C.; Brincoveanu, O.; Popescu, R.C.; Demetrescu, I. Vertical graphene growth process optimization for use in cellular identification. *Bull. Mater. Sci.* **2023**, *46*, 105. [CrossRef]
21. Mishra, K.K.; Ghosh, S.; Thoguluva, R.; Amirthapandian, S.; Kamruddin, M. Thermal conductivity and pressure-dependent Raman studies of vertical graphene nanosheets. *J. Phys. Chem. C* **2016**, *120*, 4. [CrossRef]

Disclaimer/Publisher's Note: The statements, opinions and data contained in all publications are solely those of the individual author(s) and contributor(s) and not of MDPI and/or the editor(s). MDPI and/or the editor(s) disclaim responsibility for any injury to people or property resulting from any ideas, methods, instructions or products referred to in the content.